CORE
Metadata, citation and similar papers at core.ac.uk
Provided by Online Research Database In Technology

Technical University of Denmark

On the relationship between the spherical wave expansion and the plane wave expansion for antenna diagnostics

Cappellin, Cecilia; Frandsen, Aksel; Breinbjerg, Olav

Published in:
Proceedings of the AMTA Europe Symposium

Publication date:
2006

Document Version
Publisher's PDF, also known as Version of record

Link back to DTU Orbit

Citation (APA):
Cappellin, C., Frandsen, A., & Breinbjerg, O. (2006). On the relationship between the spherical wave expansion and the plane wave expansion for antenna diagnostics. In Proceedings of the AMTA Europe Symposium

DTU Library
Technical Information Center of Denmark

General rights
Copyright and moral rights for the publications made accessible in the public portal are retained by the authors and/or other copyright owners and it is a condition of accessing publications that users recognise and abide by the legal requirements associated with these rights.

- Users may download and print one copy of any publication from the public portal for the purpose of private study or research.
- You may not further distribute the material or use it for any profit-making activity or commercial gain
- You may freely distribute the URL identifying the publication in the public portal

If you believe that this document breaches copyright please contact us providing details, and we will remove access to the work immediately and investigate your claim.

ON THE RELATIONSHIP BETWEEN THE SPHERICAL WAVE EXPANSION AND THE PLANE WAVE EXPANSION FOR ANTENNA DIAGNOSTICS

Cecilia Cappellin [1,2], Aksel Frandsen [1], Olav Breinbjerg [2]

[1] TICRA, Læderstræde 34, DK-1201 Copenhagen K, Denmark
[2] Ørsted•DTU, Technical University of Denmark, DK-2800 Kgs. Lyngby, Denmark

ABSTRACT

The relation between the plane wave expansion (PWE) and the spherical wave expansion (SWE) is investigated. It is shown how the SWE can be transformed into the PWE, from which the aperture field can subsequently be calculated. Through the SWE-PWE transformation the visible as well as the invisible regions can be recovered, providing a high spatial resolution of the aperture field.
The SWE-PWE transformation allows an efficient antenna diagnostics for spherical near-field measurements. Different test cases are examined and the limitations implied by the practical truncation of the SWE are investigated and clarified.

Keywords: Spherical near-field, Resolution, Antenna Diagnostics

1. Introduction

Electrical and mechanical errors in an antenna can be identified by use of an efficient antenna diagnostics technique. The presence of such errors is usually observed in the measured far-field pattern, however their causes can only be explained by analyzing the extreme near-field amplitude and phase. Since a direct measurement of this quantity is not usually implemented in measurement facilities, an alternative procedure has to be used. Several non-invasive diagnostics techniques have been proposed over the years [1]; however, all methods are limited either in terms of the type of antennas for which they can be used, or in terms of the accuracy that they can provide e.g. methods based on planar and cylindrical near-field or far-field measurements. There is thus a need for an antenna diagnostics technique that applies to general types of antennas, and that is intrinsically accurate. In this perspective, we propose a new technique to be applied at the DTU-ESA Spherical Near-Field Antenna Test Facility located at the Technical University of Denmark [2]. The measurement technique employed at the DTU-ESA Facility is based on the SWE of the field radiated by the antenna [3]. This expansion is mathematically valid in any source-free region of space outside the minimum sphere of the antenna, the smallest sphere centered at the origin of the measurement coordinate system which completely encloses the antenna. Thus the aperture field in the extreme near-field of the antenna can not be computed [4]. One way to overcome this is to transform the SWE of the radiated field into a PWE. We will show how the plane wave spectrum can be computed by the knowledge of the coefficients of the SWE, on any aperture plane in the antenna source-free region. This will give two main advantages. The first is that the plane wave spectrum can be evaluated also in part of the spectrally invisible region, the second is that the aperture field can be computed as an IFT of this spectrum. Hence, the spatial resolution achieved in the aperture field can in principle exceed the traditional value of half a wavelength, provided by the traditional techniques. In this manuscript analytical calculations as well as numerical simulations will be shown and investigations on the number of spherical modes necessary for the PWE convergence will be presented. All results are expressed in the S.I. rationalized system with $e^{-i\omega t}$ time convention.

2. Theory

2a) Theoretical derivation

We start by introducing the SWE of the electric field $\bar{E}$ radiated by an antenna circumscribed by a minimum sphere of radius r_o. In any source-free region $r>r_o$ the field can be expressed as [3],

$$\bar{E}(\bar{r}) = \frac{k}{\sqrt{\eta}} \sum_{n=1}^{\infty} \sum_{m=-n}^{n} Q_{1mn}^{(3)} \bar{F}_{1mn}^{(3)}(\bar{r}) + Q_{2mn}^{(3)} \bar{F}_{2mn}^{(3)}(\bar{r}) \qquad (1)$$

where $Q_{1mn}^{(3)}$ and $Q_{2mn}^{(3)}$ are the expansion coefficients, that can be obtained from a spherical near-field measurement, and $\bar{F}_{1mn}^{(3)}(\bar{r})$ and $\bar{F}_{2mn}^{(3)}(\bar{r})$ are the power-normalized spherical vector wave functions. The medium intrinsic admittance is denoted by η, k is the wave number, and $\bar{r}$ is the position vector expressed as a function of the traditional spherical coordinates (r, θ, φ). In practice, the n-summation of the SWE is truncated at $n = N$, with N usually being equal to $N = kr_o+10$. The PWE of the same electric field in the spectral $(k_x\ k_y)$-domain valid for $z>z_o$, with z_o being the largest z-coordinate of the source region, is given by [5]

$$\bar{E}(x,y,z)=\frac{1}{2\pi}\int_{-\infty}^{\infty}\int_{-\infty}^{\infty}\bar{T}(k_x,k_y)e^{ik_z z}e^{i(k_x x+k_y y)}dk_x dk_y \qquad (2)$$

where k_x, k_y, k_z are the Cartesian components of the wave propagation vector $\bar{k}$ with $k_z=\sqrt{k^2-k_x^2-k_y^2}$. The spectral domain defined by the variables k_x and k_y can be divided in two regions, the first one called "visible" for $k_x^2+k_y^2\le k^2$, responsible of the propagating plane waves, and the second one called "invisible" for $k_x^2+k_y^2>k^2$, see Fig. 1, constituted by the evanescent plane waves. The two variables (k_x k_y) are always real, while k_z is real in the visible region but purely imaginary in the invisible region. In practice, the (k_x, k_y) integrals are truncated at finite values $\pm k_{xmax}$ and $\pm k_{ymax}$.

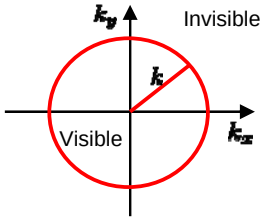

Fig.1 Visible and invisible regions in the spectral (k_x,k_y) domain.

The plane wave spectrum for a given z-coordinate is thus equal to $\bar{T}(k_x,k_y)e^{ik_z z}$. It was previously shown [6-7] how the SWE of Eq. 1 can be transformed into the PWE of Eq. 2, arriving at the following relation

$$\bar{T}(k_x,k_y)e^{ik_z z}=\frac{1}{4\pi k_z}\hat{E}(\hat{s})\,e^{ikz\cos\alpha} \qquad (3)$$

where $\hat{E}(\hat{s})$ is given by

$$\hat{E}(\hat{s})=\sum_{n=1}^{\infty}\sum_{m=-n}^{n}\frac{(-i)^n 4\pi}{\sqrt{\eta}\sqrt{n(n+1)}}\left[Q_{2mn}^{(3)}\hat{s}\times\bar{Y}_n^m(\alpha,\beta)+\right. \qquad (4)$$
$$\left.-iQ_{1mn}^{(3)}\bar{Y}_n^m(\alpha,\beta)\right]$$

with $\hat{s}=\sin\alpha\cos\beta\,\hat{x}+\sin\alpha\sin\beta\,\hat{y}+\cos\alpha\,\hat{z}$, $\beta\in[-\pi,\ \pi]$ and $\alpha\in C_+$, see Fig. 2. The vector spherical harmonics $\bar{Y}_n^m(\alpha,\beta)$ is defined by

$$\bar{Y}_n^m(\alpha,\beta)=-\frac{i}{\sqrt{2\pi}}\left(-\frac{m}{|m|}\right)^m\left(\frac{\partial}{\partial\alpha}\bar{P}_n^m(\cos\alpha)e^{im\beta}\hat{\beta}+\right. \qquad (5)$$
$$\left.-\frac{1}{\sin\alpha}\bar{P}_n^m(\cos\alpha)ime^{im\beta}\hat{\alpha}\right)$$

with $\bar{P}_n^m(\cos\alpha)$ being the normalized associated Legendre function as defined by [3], $\hat{\alpha}=\cos\alpha\cos\beta\,\hat{x}+\cos\alpha\sin\beta\,\hat{y}-\sin\alpha\,\hat{z}$ and $\hat{\beta}=-\sin\beta\,\hat{x}+\cos\beta\,\hat{y}$. The variable ($\alpha$,$\beta$) on the right hand side of Eq.3 must be expressed as functions of the spectral variables k_x and k_y according to $\hat{s}=\bar{k}/k$. The spatial resolution (δ_x,δ_y) obtained in the aperture field is given by $\delta_x=\pi/k_{xmax}$, $\delta_y=\pi/k_{ymax}$ and can thus be controlled by selecting k_{xmax} and k_{ymax} appropriately in the SWE-to-PWE transformation.

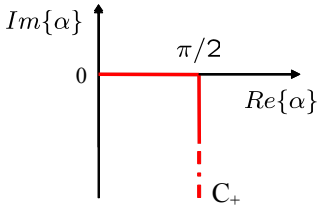

Fig.2 Domain of α variable on contour C_+.

We can therefore summarize the required steps of this antenna diagnostics technique as follows:

1. Evaluate the Q coefficients through a spherical near-field measurement of the radiated field of the AUT.
2. Calculate the plane wave spectrum in the (k_x,k_y) domain on a given z plane, $z>z_o$, according to Eqs. 3-4.
3. Compute the field on the desired z plane as the inverse Fourier transform of the spectrum through Eq. 2.

2b) Theoretical considerations

We will now focus on three specific aspects of the SWE-PWE transformation. First, by looking at the expression of the $\bar{Y}_n^m(\alpha,\beta)$ function, in Eq. 5, we see after a few mathematical manipulations that

$$\hat{s}\times\bar{Y}_n^m(\alpha,\beta)\propto\bar{K}_{2mn}(\alpha,\beta)\quad\bar{Y}_n^m(\alpha,\beta)\propto\bar{K}_{1mn}(\alpha,\beta) \qquad (6)$$

where $\bar{K}_{smn}(\theta,\varphi)=\lim_{kr\to\infty}\frac{kr}{e^{ikr}}\bar{F}_{smn}^{(3)}(r,\theta,\varphi)$ is the far-field pattern function of the spherical vector waves. We conclude that the spectrum in the (α,β)-domain, $\hat{E}(\hat{s})e^{ikz\cos\alpha}$, is thus given by the SWE of the far-field. All information about the visible and invisible spectral regions of the PWE are therefore in principle contained in the far-field. As an example of this important property, a z-oriented Hertzian dipole located at the origin of the coordinate system can be considered. Its SWE contains only the single mode s=2, m=0, n=1. From the knowledge of the corresponding coefficient $Q_{201}^{(3)}$ the plane wave spectrum is completely reconstructed in the visible as well as in the invisible region. For more realistic antennas the SWE of the field is given by a larger number of modes, however, the concept of deriving the complete set of Q's from the far-field remains

principally valid and its consequences will be discussed more later. Second, since the variable α becomes purely imaginary in the invisible domain, see Fig.2, the trigonometric functions in α included in $\overline{Y}_n^m(\alpha,\beta)$ are not limited in that region, and this gives rise to computational problems already for moderate values of n. An example is shown in Fig.4, where the amplitude of the spectrum on $z=\lambda$ for s=1, m=0 and n= 20 and $Q_{1020}^{(3)}=1$ is presented in logarithmic scale and normalized to the value on axis.

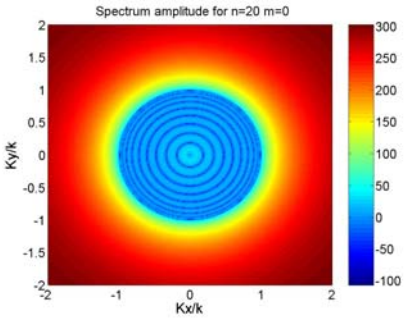

Fig.4 Amplitude of the spectrum for n=20, m=0 on $z=\lambda$, in dB.

On the other hand, the exponential term $e^{ik_z z}$, which is also included in the spectrum, provides a decay in the invisible domain. A way to partly control the computational difficulties is therefore to embed the term $e^{ik_z z}$ into the calculation of the vector spherical harmonics. Third, we will concentrate on Eq. 3. It is noted that a singularity for k_z=0 ($k_x^2+k_y^2=k^2$) will always be present at least in one component of any antenna spectrum, and that the necessary but not sufficient condition to avoid that is that the antenna far-field pattern presents a null for $\theta=\pi/2$ [5]. The singularity prevents a direct use of the IFT for the calculation of the aperture field, since an infinite number of points would be required to correctly sample the function in the vicinity of k_z=0. But there is a way to overcome the problem and get an accurate value of the field even from components affected by the singularity. For this purpose, we write the spectrum $\overline{T}$ as a product of two functions, $\overline{T}_1$ with no singularity, and $1/k_z$, i.e. $\overline{T}(k_x,k_y)=\overline{T}_1(k_x,k_y)\dfrac{1}{k_z}$. We know that the IFT of $\overline{T}$ is the convolution in the spatial (x,y,z) domain of the IFT's of the two separated functions. We inverse transform with an IFT $\overline{T}_1$ and we write the inverse Fourier transform of $1/k_z$ by use of the Weyl identity [5] for $z>0$

$$\frac{e^{ikr}}{i2\pi r}=\frac{1}{2\pi}\int_{-\infty}^{\infty}\int_{-\infty}^{\infty}\frac{1}{k_z}e^{i(k_x x+k_y y+k_z z)}dk_x dk_y \qquad (6)$$

To properly convolve $\bar{t}_1(x,y,z)=\mathrm{F}^{-1}\{\overline{T}_1(k_x,k_y,\mathrm{z})\}$ with the Green function, we need to split the quantity z in two, $z=z+z_1-z_1$, to have an exponential factor of the type of $e^{ik_z z}$ on both terms. We get

$$\mathrm{F}^{-1}\{\overline{\mathrm{T}}(\mathrm{k_x},\mathrm{k_y})\}=\bar{t}(x,y,z)=t_1(x,y,z-z_1)\otimes\frac{e^{ikr_1}}{i2\pi r_1} \qquad (7)$$

with $r_1=\sqrt{x^2+y^2+z_1^2}$. Since in the practice we deal with functions defined on a discrete domain of finite dimension, we need to implement a circular convolution, according to the discrete Fourier transform theory described in [8]. The results and the accuracy of this method will be shown in the following section, dedicated to the test cases.

3. Test Cases

3a) Array of Hertzian dipoles

A set of five x-oriented Hertzian dipoles on the x-y plane, four equally displaced from the origin with the distance r_o and one at the center, see Fig.5, is the first test case.

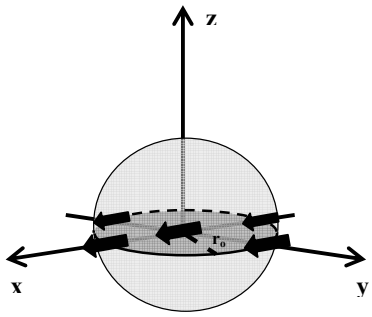

Fig.5. Five Hertzian dipoles displaced on the x-y plane, with minimum sphere of radius r_o.

With such a configuration, the aperture plane can be moved into the minimum sphere of radius r_o, still remaining in a source-free region. For this antenna the Q coefficients can be calculated analytically, by use of the results reported in [3, pp. 339] for a sampled x-polarized planar current ring. Since the SWE contains arbitrarily high-order modes in n and m, the influence of the truncation in n in Eq. 4 can be analyzed. We consider as reference spectrum the one calculated through the dipole currents [5]

$$T_x=\frac{P\sqrt{\mu}}{2\pi k\sqrt{\varepsilon}}\left(\cos(k_x r_o)+\cos(k_y r_o)+\frac{1}{2}\right)\frac{k_x^2-k^2}{k_z} \qquad (8)$$

$$T_y=\frac{P}{2\pi k}\sqrt{\frac{\mu}{\varepsilon}}\left(\cos(k_x r_o)+\cos(k_y r_o)+\frac{1}{2}\right)\frac{k_x k_y}{k_z}$$

$$T_z=\frac{P}{2\pi k}\sqrt{\frac{\mu}{\varepsilon}}\left(\cos(k_x r_o)+\cos(k_y r_o)+\frac{1}{2}\right)k_x$$

with P being the dipole moment. T_x and T_y contain the singularity in k_z. Different values of r_o have been studied, and here the results for $r_o = 2\lambda$ corresponding to kr_o=12, will be considered. The spectral components are then computed with Eq.4 for different values of N. The plots for $N=kr_o$, $N=kr_o+10$, $N=kr_o+40$ for the x-component on $z=0.2\lambda$ are shown in dB in Fig.6, normalized to the value of T_x in the origin. We see how the convergence region in the (k_x,k_y) domain increases gradually with increasing N. For $N=kr_o$ the visible region is still not completely reconstructed but its convergence is reached with $N=kr_o+10$. For $N>kr_o+10$, only changes in the invisible region are noted until the complete picture obtained by $N=kr_o+40=52$. The singularity for $k_z=0$ is perfectly identified, already by $N=kr_o+10$.

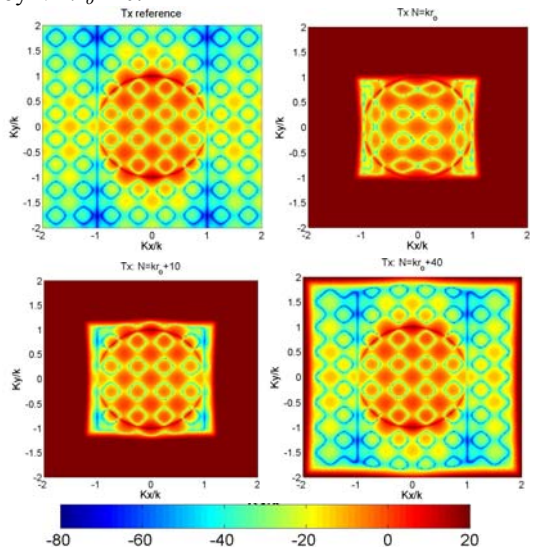

Fig.6 Amplitude of the x component of the spectrum of the five dipoles with $r_o=2\lambda$, on $z=0.2\lambda$ in dB: the reference T_x, $N=kr_o$, $N=kr_o+10$ and $N=kr_o+40$.

To better understand the convergence mechanism, we also plot the n-mode power spectrum, $P_{rad}(n)=\frac{1}{2}\sum_{sm}\left|Q^{(3)}_{smn}\right|^2$ in function of n, see Fig.7. Extreme low values of power are contained in the high n modes, however, due to the corresponding low values of Q's the product with the diverging vector spherical harmonics is kept finite. A plot of the x component of the spectrum in function of N, for different points of the spectral domain, can finally clarify the convergence mechanism, see Fig.8. Points belonging to the visible region reach the convergence with $N=kr_o+10$, while points in the invisible domain need more modes as they move away from the visible domain. The maximum N required for a complete convergence in the $(-2k,2k)$ domain depends on r_o. It has been found that generally $N=kr_o+4kr_o$ is needed for the five dipoles case. From Fig.8 we see that the series behaves as one with alternating sign. At every step n a new quantity is summed to the previous terms, adding or subtracting a certain amount of spectrum.

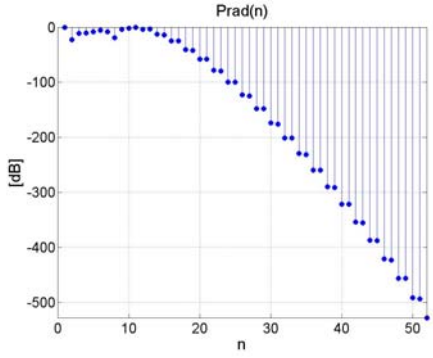

Fig.7 n-mode power spectrum for $r_o=2\lambda$.

This is necessary in order to "clean" the spectral invisible region, until the convergence values are reached.

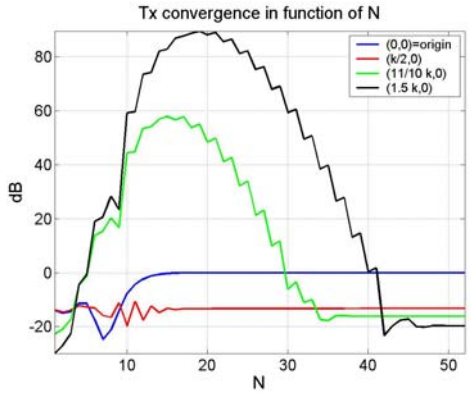

Fig.8 Amplitude of the x component of the spectrum in function of N, kr_o=12, for different points of the spectral domain.

We can therefore inverse Fourier transform the spectrum and compare the quantity with the analytical field. Since the spectral domain has an extension of $(-2k,2k)$, the resolution achieved in the (x,y) domain is equal to $\lambda/4$. The z component can be directly inverse Fourier transformed, while the x and y components require the procedure of the circular convolution. To understand the influence of the invisible region, we consider the spectrum computed with $N=kr_o+40=52$, $N=kr_o+10=22$ and $N=kr_o=12$. Only the convergent part of the spectrum was used in these cases, while the non-convergent part was replaced by zeros. Results are shown in Fig.9 for the x component on $z=0.2\lambda$. The figures are normalized to the value on axis of the analytical field and plotted in linear scale: we can distinguish the five dipoles on the (x,y) plane in all pictures. However the result provided by $N=kr_o$ is not quantitatively satisfactory in determining the dipoles contribution. On the other hand, already

with $N=kr_o+10$ terms a very accurate aperture field is computed. This means that the most important part of the spectrum to be recovered is constituted by the visible region, the singularity for $k_z=0$, and a little part of the invisible region.

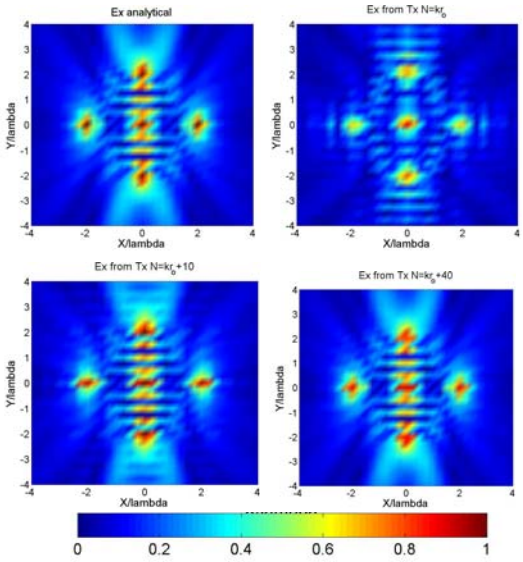

Fig.9 Amplitude of the *x* component of the field on $z=0.2\lambda$, for $r_o=2\lambda$ in linear scale: the analytical, the one obtained by $N=kr_o$, $N=kr_o+10$ and $N=kr_o+40$.

3b) Rectangular aperture in free-space

The second antenna test case is a rectangular aperture with the TE01 mode, located on the *x-y* plane and radiating in free space, see Fig. 10.

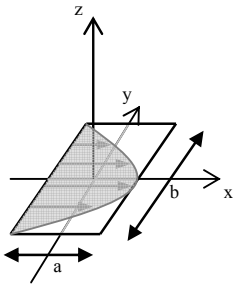

Fig.10 Rectangular aperture, of dimension *a* and *b*, located on the *x-y* plane, with mode TE01.

From the analytical far-field pattern $\overline{F}(\theta,\varphi)$, based on electrical and magnetical equivalent currents [9], the reference spectrum $\overline{T}$ is calculated as $\overline{T}(k\sin\theta\cos\varphi, k\sin\theta\sin\varphi)=\frac{i\overline{F}(\theta,\varphi)}{k\cos\theta}$ [5], with $\theta\in[0,\pi/2]$ and $\varphi\in[0,2\pi)$. This immediately provides the expression for $\overline{T}$ in the visible domain $k_x^2+k_y^2\le k^2$. However it is possible to analytically continue the far-field pattern $\overline{F}(\theta,\varphi)$ to complex values of θ [5], so that by the use of the same expression the spectrum $\overline{T}$ in the invisible domain is also calculated. The angle θ will be substituted by α defined on the domain C_+ and φ by β. The Q coefficients are calculated from the projection of the far-field on the functions $\hat{s}\times\overline{Y}_n^m(\alpha,\beta)$ and $\overline{Y}_n^m(\alpha,\beta)$, but due to numerical problem, only $N=19$ terms are available. Different values of a and b have been analyzed, and here we present the results for $a=\lambda$ and $b=2\lambda$, corresponding to $kr_o=6$. The expressions of the reference spectral components are:

$$T_x=\frac{abk}{4k_z}\frac{\cos Y}{Y^2-(\pi/2)^2}\frac{\sin X}{X}\left(\frac{k_z k_x^2}{k(k_x^2+k_y^2)}\left(1+\frac{\beta_{01}k_z}{k^2}\right)+\frac{k_z k_y^2}{k(k_x^2+k_y^2)}\left(1+\frac{\beta_{01}}{k_z}\right)\right) \quad (9)$$

with $\beta_{01}/k=\sqrt{1-(\lambda/(2b)^2)}$, $X=k_x a/2$, and $Y=k_y b/2$ with $T_y=0$ and $T_z=-k_x T_x/k_z$, from $\overline{k}\cdot\overline{T}=0$. The singularity in $k_z=0$ is present both in T_x and T_z. Again we will calculate the spectrum through Eq.4 with different value of N, and we will focus on the x component, see Fig.11 where the quantities are normalized to the value of T_x in the origin and plotted on $z=0.2\lambda$. The convergence mechanism is similar to the one shown by the five dipoles case.

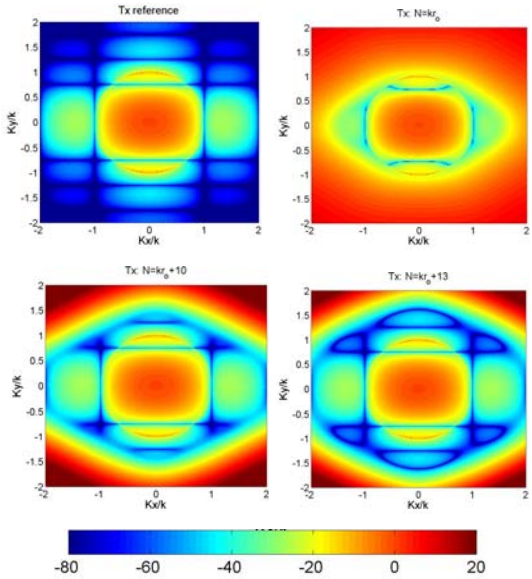

Fig.11 Amplitude of the *x* component of the spectrum for the rectangular aperture with $a=\lambda$ and $b=2\lambda$, on $z=0.2\lambda$ in dB: the reference T_x, $N=kr_o$, $N=kr_o+10$ and $N=kr_o+13$.

As before, the singularity on k_z=0 is perfectly identified. Slightly more than kr_o terms are needed for the convergence of the visible region, while modes with $n>kr_o$ have influence on the invisible domain. The n-mode power spectrum is reported in Fig. 12, and compared to the one of a set of five dipoles with $r_o=\lambda$ and thus the same value of kr_o. The power contained in the high n modes is lower than in the five dipoles case: the corresponding Q's can therefore better control the product with the diverging vector spherical harmonics. This could be the reason why a large part of the invisible region is reconstruct already for $N= kr_o+10$.

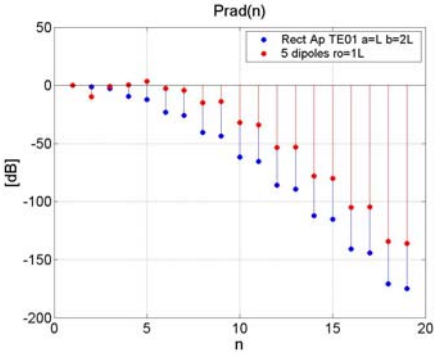

Fig.12 *n*-mode power spectrum for a rectangular aperture with $a=\lambda$ and $b=2\lambda$, compared with the one given by five dipoles with the same r_o.

The x component of the field is finally calculated on $z=0.2\lambda$ as inverse Fourier transform of the x component of the spectrum with the use of the circular convolution, see Fig.13. No analytical expression of the field is known on that z plane, so the comparison is done between the IFT of the reference spectrum and the IFT of the spectrum represented by $N=kr_o+10$ terms, with the non-converging region replaced by zeros. Results are in linear scale and normalized in respect to the value on axis of the field obtained by the reference spectrum. The aperture dimensions on the (x,y) plane are identified, and again, extremely good agreement is found between the two pictures.

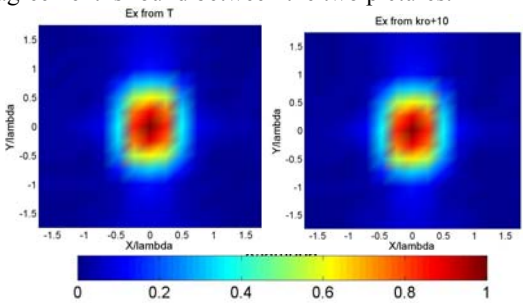

Fig.13 Amplitude of the x component of the field on $z=0.2\lambda$, for a rectangular aperture with $a=\lambda$ and $b=2\lambda$, in linear scale: on the left from the reference spectrum, on the right from $N=kr_o+10$.

Conclusions

A new antenna diagnostics technique for spherical near-field antenna measurements has been presented. The theoretical derivations as well as the two test cases have shown an important property: the plane wave spectrum, in the visible as well as in part of the invisible region, can be derived by the knowledge of the Q coefficients of the SWE of the field. This provides a spatial resolution in the aperture field higher than the usual half wavelength provided by the traditional techniques. It is important to point out that, while the reconstruction of the invisible domain of the PWE is in principle possible from the SWE, the practical truncation of the SWE in real measurements will of course enforce a limitation on this. However, it has been shown that very accurate aperture fields can be obtained with a realistic truncation number, provided that the k_z=0 singularity of the PWE is recovered. Future work will focus on the influence of noise and finite dynamic range on the truncation number for different types of antennas. Real measured data will then be included in the analysis.

8. REFERENCES

[1] Kaplan L., Hanfling J. D., Borgiotti G. V., *The Backward Transform of the Near-Field for Reconstruction of Aperture Field,* IEEE Trans. on Ant. and Prop. Soc. Symp. Dig., 764-767, 1979.

[2] Homepage of the DTU-ESA Facility: http://www.oersted.dtu.dk/English/research/emi/afg/dtu_esa_facility.aspx

[3] Hansen J. E., *Spherical Near-Field Antenna Measurements*, Peter Peregrinus Ltd. London, 1988.

[4] Joy E. B., Guler M. G., *High Resolution Spherical Microwave Holography*, IEEE Trans. on Ant. and Prop., vol. 43, 464-472, 1995.

[5] Hansen T. B., Yaghjian A. D., *Plane Wave Theory of Time-Domain Fields, Near-Field Scanning Applications*, IEEE PRESS, 1999.

[6] Devaney A. J., Wolf E., *Multipole Expansion and Plane Wave Representations of the Electromagnetic Field*, Journal of Math. and Physics, Vol. 15, 234-244, February 1974.

[7] Cappellin C., Breinbjerg O., Frandsen A., *A high Resolution Antenna Diagnostics Technique for Spherical Near-Field Measurements,* 28th ESA Antenna Workshop, ESTEC, Noordwijk, The Netherlands, pp 899-906, 2005.

[8] Oppenheim A. V., Schafer R. W., *Digital Signal Processing*, Prentice-Hall, 1975.

[9] Silver S., *Microwave Antenna theory and Design,* Peter Peregrinus Ltd. London, 1984.